Available online at www.sciencedirect.com
ScienceDirect
Journal of Molecular Graphics and Modelling 26 (2007) 471–481
Journal of Molecular Graphics and Modelling
www.elsevier.com/locate/JMGM

Molecular dynamics at the receptor level of immunodominant myelin basic protein epitope 87–99 implicated in multiple sclerosis and its antagonists altered peptide ligands: Triggering of immune response

Efthimia D. Mantzourani [a,b], James A. Platts [c], Andrea Brancale [d], Thomas M. Mavromoustakos [a], Theodore V. Tselios [b,*]

[a] *Institute of Organic and Pharmaceutical Chemistry, National Hellenic Research Foundation, 48 Vassileos Constantinou Avenue, 116 35 Athens, Greece*
[b] *Department of Chemistry, University of Patras, 265 00 Rion, Patras, Greece*
[c] *School of Chemistry, Cardiff University, CF10 3AT Cardiff, UK*
[d] *Welsh School of Pharmacy, Cardiff University, Redwood Building, King Edward VII Avenue, CF1 3XF Cardiff, UK*

Received 11 January 2007; received in revised form 14 February 2007; accepted 20 February 2007
Available online 23 February 2007

Abstract

This work reports molecular dynamics studies at the receptor level of the immunodominant myelin basic protein (MBP) epitope 87–99 implicated in multiple sclerosis, and its antagonists altered peptide ligands (APLs), namely [Arg^{91}, Ala^{96}] $MBP_{87–99}$ and [$Ala^{91,96}$] $MBP_{87–99}$. The interaction of each peptide ligand with the receptor human leukocyte antigen HLA-DR2b was studied, starting from X-ray structure with pdb code: 1ymm. This is the first such study of APL-HLA-DR2b complexes, and hence the first attempt to gain a better understanding of the molecular recognition mechanisms that underlie TCR antagonism by these APLs. The amino acids His^{88} and Phe^{89} serve as T-cell receptor (TCR) anchors in the formation of the trimolecular complex TCR-peptide-HLA-DR2b, where the TCR binds in a diagonal, off-centered mode to the peptide-HLA complex. The present findings indicate that these two amino acids have a different orientation in the APLs [Arg^{91}, Ala^{96}] $MBP_{87–99}$ and [$Ala^{91,96}$] $MBP_{87–99}$: His^{88} and Phe^{89} remain buried in HLA grooves and are not available for interaction with the TCR. We propose that this different topology could provide a possible mechanism of action for TCR antagonism.

Keywords: Molecular dynamics; Peptides; Receptors; Molecular recognition; Altered peptide ligands

1. Introduction

The immune system is designed to detect the unwanted presence of invaders, such as bacteria, parasites or viruses, by continuous sampling of the proteins present both inside and outside the cells of the body. This is achieved by breaking these proteins down into short peptides and loading them on to specialized carriers, the major histocompatibility complex (MHC) molecules [1]. MHC molecules capture and display such peptides on the surface of antigen-presenting cells (APCs). These bound peptide – MHC complexes (pMHC) are scrutinized by T-lymphocytes via their T-cell receptor (TCR) during immunosurveillance [2]. Since T-cells recognizing self-peptides are eliminated during the process of thymic selection, those pMHC incorporating foreign peptides are the primary focus of T-cell mediated immune responses [3,4].

In the human, MHC molecules are referred to as HLA (Human Leukocyte Antigens), and are encoded by the chromosome 6p21.3-located HLA region [5]. A robust association has been established between Multiple Sclerosis (MS), an autoimmune, inflammatory disease whose etiology still remains unknown, and alleles of the MHC complex, for haplotypes representing types of the MHC II molecules [6]. Even though susceptibility to MS is probably mediated by a heterogeneous array of genes [7], previous studies have demonstrated that the HLA-DR2b (DRB1*1501) haplotype

* Corresponding author. Tel.: +30 2610 997905; fax: +30 2610 997180.
E-mail addresses: efi_mantz@yahoo.gr (E.D. Mantzourani), platts@cardiff.ac.uk (J.A. Platts), brancalea@cf.ac.uk (A. Brancale), ttselios@upatras.gr (T.V. Tselios).

1093-3263/$ – see front matter © 2007 Elsevier Inc. All rights reserved.
doi:10.1016/j.jmgm.2007.02.004

is present at an increased frequency in northern European Caucasoid patients with MS [8,9].

MHC II molecules are heterodimers comprised of two subunits, each with a single membrane-spanning anchor [10]. The extracellular segment of the α chain includes α1 and α2 domains, and likewise, the β chain is composed of β1 and β2 domains. In the mature MHC II molecule, the α2 and β2 domains fold as independent immunoglobulin (Ig)-like domains, whereas α1 and β1 fold together, creating a single antigen-presenting platform. It is in this platform that antigenic epitopes bind, TCRs recognise them and an immunologic response is triggered. Although the antigenic components of myelin in MS have not been identified with certainty yet, myelin basic protein (MBP) is believed to be one of the main autoantigens and $MBP_{87–99}$ is encephalitogenic in experimental autoimmune encephalomyelitis (EAE), the best studied animal model for MS [11–15].

The ability of a pMHC complex to activate a T-cell generally correlates with the strength and duration of TCR binding [16]. High affinity of TCR for the pMHC, and long half-lives of binding have been associated with agonist action, whereas low affinity of TCR for the pMHC, with weak interactions formed and decreased half-lives of binding characterize TCR antagonism. The TCR is an αβ heterodimeric molecule consisting of variable and constant Ig domains in which the complementarity determining regions (CDRs) of the variable domains comprise the peptide-MHC binding surface. A two-step mechanism for TCR recognition has been proposed [17]. Initial TCR-MHC interactions, aided by TCR contacts with the peptide, guide the TCR to its ligand in an orientation that positions CDR1 and CDR2 loops mainly over the MHC. This is followed by a final folding of the two CDR3 loops of the TCR over the peptide. T-cell activation is triggered only on the formation of stable peptide contacts and agonists deliver specific signals. Antagonism requires an altered peptide ligand (APL) to induce bioachemical activity which is inhibitory over the agonist-delivered signals. CDR3 loops of TCR are highly flexible and mobile in the unbound state [18] and adopt conformations that cannot specifically contact peptide residues without substantial rearrangement. In contrast, the CDR1 and CDR2 loops are much more rigid, generally showing little or no rearrangement on binding peptide-MHC. Thus, the TCR may scan MHC molecules using a ‘‘lock and key’’ type of binding with its CDR1 and CDR2 loops, followed by an induced fit of its CDR3 loops over the peptide [19].

The crystal structure of HLA-DR2b (DRA, DRB1*1501) was determined by Smith et al., [20] complexed with $MBP_{83–97}$ (Scheme 1), a peptide from human MBP that was found to be immunodominant. Val^{87} and Phe^{90} of the $MBP_{83–97}$ peptide were the primary P1 and P4 anchors for HLA-DR2b binding. Also, Asn^{92} binds in a polar P6 pocket. Side chains of Ile^{93} and Thr^{95} bind in pockets P7 and P9 respectively. The numbering of the amino acids in the peptide follows the convention in the field in which the residue in the first HLA pocket is 1, and N-terminal residues are −1, −2 etc. P2 His^{88}, P3 Phe^{89}, and P5 Lys^{91} were solvent exposed residues, and identified as TCR contacts. Hahn et al. [21] have reported the crystal structure (PDB code 1ymm) of the trimolecular complex of $MBP_{83–96}$, HLA-DRB1*1501, and a human TCR isolated from a patient with relapsing-remitting MS [22,23]. The conformation of the pMHC complex in the two crystal structures is very similar ($RMSD_{Ca–C–N}$: 0.515). This TCR represents one of the best-characterized TCRs from a human autoimmune disease, and presents a topology notably different from that of antimicrobial ones [24–26]. Li et al. [27] have isolated the complex of a human autoimmune TCR with HLA-DR2a, where Phe^{89}, Lys^{91}, Val^{94} and Pro^{96} serve as TCR contact residues. Both human autoimmune TCRs contact only the N-terminal region of the peptide rather than being centred on the peptide-MHC complex, with the one in complex with HLA-DR2b specifically contacting the residues P2 His^{88} and P3 Phe^{89}. The N-terminus of the peptide arches up at the TCR, which contacts the peptide at the Glu at position −4. It is believed that the aberrant binding properties increase the probability that autoreactive T cells escape deletion in the thymus and attack self-myelin.

We used the pMHC complex from the latter crystal structure for our studies of the binding of HLA to two APLs of the immunodominant $MBP_{87–99}$ that have already been tested and proved to inhibit EAE induced by guinea pig $MBP_{74–85}$ epitope [28], namely antagonists. $MBP_{87–99}$ was found to induce EAE, *i.e.* to be an agonist, and NMR conformational studies revealed that one of the most abundant populations present in solution is similar to the sequence 87–97 isolated from $MBP_{83–97}$ of the crystal structure [29]. Therefore, this is likely to be the conformation with which it binds to the receptor and causes the immunological response. Thus, comparisons of the APL-HLA complexes to the X-ray structure can be made, in order to derive conclusion regarding the antagonistic activity. To our knowledge, no other study of APL-HLA-DR2b complexes has been published, and hence this is the first attempt to provide a deeper understanding of the molecular recognition mechanisms that underlie the suppression of EAE by these APLs.

The 3D structures of the linear APLs [Arg^{91}, Ala^{96}] $MBP_{87–99}$ and [$Ala^{91,96}$] $MBP_{87–99}$ (Scheme 1) in solution have already been described [30,31]. Putative bioactive conformations have been proposed, *i.e.* conformations that would enable binding with the HLA, but fail to activate the TCR and therefore to trigger an immune response. These conformations were used in the present study as starting points for interaction with the HLA-DRB1*1501. It is known that flexible molecules are deformed when binding to proteins [32], but it is important to use as an initial conformation one that the molecule can actually adopt in solution and not one that arises after theoretical calculations only. The APL-MHC complexes were then subjected to molecular dynamics simulation (MD) in solvent, including all domains of the receptor [33], and the same procedure applied to the $MPB_{83–96}$ – MHC complex, thus allowing direct comparison of results for agonist (EAE-inducing) and antagonist peptides (EAE-preventing) and providing a possible explanation of EAE antagonism. Attachment to the peptide-binding groove of MHC is due to a network of hydrogen bonds between the peptide backbone and the active site, and by hydrophobic interactions of peptide side chains and the pockets of the binding site. These bonds and interactions

were studied over the course of MD simulation, and the solvent accessible surface area (SASA) of the bound peptides calculated. From these calculations, a structural motif for antagonistic activity was sought, which could ultimately lead to rational design of potent non-peptide mimetic compounds, active against MS.

Scheme 1: Primary sequence of the peptides under study. The first residue of the two epitopes was labelled Val^{87} according to Karin et al. [34]. The numbering of the pdb structure is according to Medline Unique Identifier (UID), and it should be shifted by two residues (Val^{87} of $MBP_{87–99}$ is equal to Val^{89} of the pdb structure [35]). For simplicitly reasons in this paper we are using only one way of numbering

$MBP_{83–97}$:	Glu^{83}-Asn^{84}-Pro^{85}-Val^{86}-Val^{87}-His^{88}-Phe^{89} -Phe^{90}-Lys^{91}-Asn^{92}-Ile^{93}-Val^{94}-Thr^{95}-Pro^{96}-Arg^{97}
$[Arg^{91},Ala^{96}]MBP_{87–99}$:	Val^{87}-His^{88}-Phe^{89}-Phe^{90}-Arg^{91}-Asn^{92}-Ile^{93} -Val^{94}-Thr^{95}-Ala^{96}-Arg^{97}-Thr^{98}-Pro^{99}
$[Ala^{91,96}]MBP_{87–99}$:	Val^{87}-His^{88}-Phe^{89}-Phe^{90}-Ala^{91}-Asn^{92}-Ile^{93} -Val^{94}-Thr^{95}-Ala^{96}-Arg^{97}-Thr^{98}-Pro^{99}

2. Methodology

2.1. Molecular dynamics (MD)

All peptide–protein MD simulations were performed with GROMACS 3.2 [36,37], applying GROMOS96 [38] and ffG43a1 force field. The leap-frog algorithm [39] was used to integrate the equations of motion. LINCS algorithm [40] was incorporated to impose constraints on bonds and angles, after an unconstrained update. GROMACS atom types were used throughout [41–46].

The system was solvated by a space-filling box, which is surrounded by translated copies of itself, thus applying periodic boundary conditions and minimizing edge effects, using the simple point charge spc216 water model [47]. A triclinic unit cell was used [48], and the distance of the system from the cell edge (image distance) was 9 Å. Periodic boundary conditions were combined with the minimum image convention, and for long-range electrostatic interactions PME [49,50] lattice sum method was incorporated, using a cubic interpolation (4th order). The charges were assigned to a grid, which was then Fourier transformed with a 3D FFT algorithm, using a maximum spacing for the FFT grid of 1.2 Å.

Internal forces at any given time were calculated as non-bonded interactions generated from a dynamic list of pairs of atoms (neighbor list). The cutoff for short-range neighbor list was 9 Å, and the pair list was updated every 5 steps. Neighbor searching was performed involving periodic boundary conditions, and a grid search. Electrostatic cut-off was 9 Å, van der Waals cut-off was 14 Å. The simulation temperature was 300 K, controlled with the extended ensemble Nose–Hoover scheme [51,52] to enable canonical ensemble simulations.

Initial energy minimization was done using Steepest–Descent algorithm for 1 ps, followed by a position-restrained MD for 20 ps in order to equilibrate the water around the system and make it homogeneous. Initial velocities were generated according to a Maxwell distribution at 300 K with random seed generator. An MD simulation was then performed for 2 ns, using a time step for all calculations of 2 fs.

All simulations were performed on a Beowulf cluster [53] using 16 parallel processors. The trajectories generated were viewed with VMD [54], coordinates of all frames were saved as pdb files, and were analyzed with MOE 2005.06 by Chemical Computing Inc. [55] on a RM 3 GHz Pentium IV workstation.

3. Results and discussion

3.1. Structural characteristics of $MBP_{83–96}$ complexed with HLA-DR2b and TCR (pdb code: 1ymm[20])

Scoring.svl [56] in MOE was used as a tool for analysis and visualization of direct hydrogen bonds and other non-bonded intermolecular interactions in the X-ray structure. The results are presented in Tables 1–3. Each hydrogen bond identified is characterised by a ''relative strength'' percentage, relative to an ''ideal'' hydrogen bond of that type, as computed by the scoring function of the algorithm. The distance between the two atoms forming the bond is also calculated. Other non-bonded intermolecular interactions are also calculated between the ligand and the remainder of the system, *i.e.* van der Waals dispersion forces and dipole–dipole interactions. The atom names shown are those employed by MOE and are reported in supporting information.

Due to the orientation of binding of the TCR to the peptide-HLA-DR2b complex, there are no contacts whatsoever of the sequence 92–96 with the TCR (Table 3). Several non bonded intermolecular interactions appear between Vα and Vβ chains of TCR and the first four amino acids of the ligand, *i.e.* those that are engineered out of the APLs. One of the two hydrogen bonds formed (Table 1) also involves one of these amino acids, Val^{88}, and Vα. The other hydrogen bond is formed between Phe^{91} and Vβ. A network of weaker non-bonded interactions is

Table 1
Network of hydrogen bonds formed between $MBP_{83–96}$ and the proteins HLA-DR2b and TCR in crystal structure. Vα and Vβ are the chains of the TCR molecule, and α and β are the chains of HLA-DR2b

Ligand atom		Protein atom		Relative strength (%)	Distance (Å)
Hydrogen bonds					
H(N)	Val^{86}	O	Vα Gly^{96}	73	3.0
H(N)	Val^{87}	O	α Ser^{53}	85	2.9
H(ND1)	His^{88}	O	β Thr^{77}	4	3.8
O	His^{88}	H(ND2)	β Asn^{82}	13	2.9
O	Phe^{89}	H(N)	V β Ala^{103}	84	2.9
H(N)	Phe^{90}	OE1	α Gln^{9}	80	2.7
O	Phe^{90}	H(NE2)	α Gln^{9}	40	3.2
O	Phe^{90}	H(ND2)	α Asn^{62}	14	3.4
H(N)	Asn^{92}	OD1	α Asn^{92}	100	2.6
OD1	Asn^{92}	H(N)	β Arg^{13}	56	2.5
H(ND2)	Asn^{92}	OE1	α Glu^{11}	51	2.8
H(ND2)	Asn^{92}	O	α Asn^{62}	78	2.6
H(ND2)	Asn^{92}	OD2	α Asp^{66}	3	3.6
O	Ile^{93}	H(ND2)	α Asn^{69}	10	3.4
O	Val^{94}	H(NE2)	α Trp^{61}	60	3.0
H(N)	Thr^{95}	OD2	α Asn^{69}	67	3.0

Table 2
Network of non-bonded intermolecular interactions between the sequence 87–95 of $MBP_{83–96}$ and HLA-DR2b in crystal structure. α and β are the chains of HLA-DR2b

Ligand residue	Protein residue				
Val^{87}	α Ile^{7}	α Phe^{24}	α Ile^{31}	αPhe^{32}	α Trp^{43}
	βAsn^{82}	β Val^{85}	β Val^{86}	βPhe^{89}	
His^{88}	αPhe^{54}	β Tyr^{78}	β His^{81}		
Phe^{89}	αPhe^{22}	α Phe^{24}	α Phe^{32}	αPhe^{54}	α Gly^{58}
	α Ala^{59}	α Ala^{61}	α Asn^{62}	β Tyr^{78}	
Phe^{90}	α Gln^{9}	β Arg^{13}	β Phe^{26}	βPhe^{40}	β Phe^{47}
	β Gln^{70}	β Ala^{71}	β Tyr^{78}		
Lys^{91}	α Val^{65}				
Asn^{92}	α Val^{65}				
Ile^{93}	α Val^{65}	β Tyr^{30}	β Phe^{47}	β Tyr^{60}	β Trp^{61}
	β Gln^{64}	β Ile^{67}			
Val^{94}	α Val^{65}	α Ala^{68}	β Tyr^{60}	β Ile^{67}	α Ile^{72}
Thr^{95}	α Ile^{72}	α Met^{73}	β Trp^{9}	β Tyr^{60}	β Trp^{61}

Non-bonded intermolecular interactions (sequence 87–95) with HLA-DR2b.

Table 3
Network of non-bonded intermolecular interactions between $MBP_{83–96}$ and TCR in crystal structure. Vα and Vβ are the chains of the TCR molecule

Glu^{83}	Vα Thr^{97}	Vβ Lys^{55}	Vβ Tyr^{58}	
Asp^{84}	Vα Thr^{97}			
Pro^{85}	Vα Gly^{96}	Vα Thr^{97}		
Val^{86}	Vα Gly^{96}	Vα Thr^{97}	Vα Tyr^{98}	Vβ Arg^{97}
Val^{88}	Vα Tyr^{98}			
His^{88}	Vβ Gly^{102}	Vβ Ala^{103}	Vβ Asn^{104}	
Phe^{89}	Vβ Leu^{99}	Vβ Thr^{100}	Vβ Gly^{102}	
Phe^{90}	Vβ Ala^{103}			
Lys^{91}	Vβ Thr^{100}	Vβ Ala^{103}		

Non-bonded intermolecular interactions with TCR.

present (Table 2) involving the amino acid sequence common to our peptides as well, starting from Val^{87}.

3.2. Molecular dynamics of $MBP_{83–96}$ complexed with HLA-DR2b

MD simulation of the native ligand bound to HLA-DR2b has been performed for comparison with the complexes of the two APLs with the latter. This allows us to trace conformational changes, and to determine an average conformation against which APL structures can be compared. The crystal structure of $MBP_{83–96}$ complexed with HLA-DR2b [21] was used as the starting point for MD simulation. The energy of the system at each time step of the trajectory was calculated and the ten lowest energy frames were selected, thus avoiding the risk of getting stuck in a restricted time period and achieving a better distribution of the sampling of the whole system. The peptides were isolated from the complexes, and superimposed onto the conformation in the X-ray structure. Fig. 1 shows these low energy conformations superimposed on the Gauss–Connolly surface of the protein calculated using 0.75 Å grid and 1.4 Å probe radius. Exposed parts are coloured in red, hydrophilic in blue, and hydrophobic in green. A side view of this superimposition of the peptides, as well as one using the trimolecular complex, is presented in supporting information.

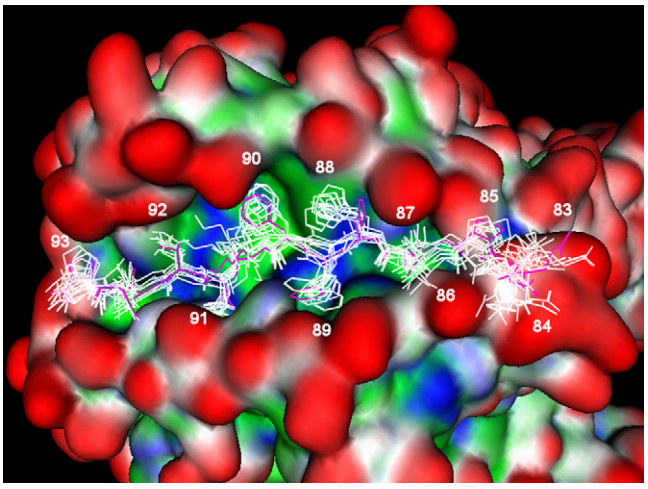

Fig. 1. Superimposition of the $MBP_{83–96}$ conformations in the ten lowest energy frames onto the X-ray structure of the peptide-HLA-DR2b complex after MD simulations. Exposed parts are coloured in red, hydrophilic in blue, and hydrophobic in green. The conformation of the native peptide is coloured purple.

The Cα RMSD is 1.09 Å averaged over the ten structures, implying that the backbone of the peptides does not vary significantly. Fig. 1 also shows that the side chains of the N-terminus of the peptide, *i.e.* residues Glu −4, Asn −3, Pro −2, and Val −1 fluctuate, as they are exposed to the solvent and can move freely. The same is observed for the other exposed residues: His^{88}, Lys^{91}, Val^{94}, and Pro^{96}. Especially for His^{88} this flexibility is expected, as in the crystal structure it interacts with TCR, whereas in this simulation solvent surrounds it. As a result, the intermolecular contacts are absent, and dihedral angle χ1 changes so that the imidazole ring orientates towards a lower energy conformation. To quantify the alteration in exposed and buried residues, we calculated the Solvent Accessible Surface Area (SASA) employing the GETAREA algorithm [57,58], which calculates total surface area, with individual contributions from apolar, backbone, and side-chain parts. A ratio per residue is given between the side-chain surface area and the ''random coil'' value. The ''random coil'' value of a residue X is the average solvent-accessible surface area of X in the tripeptide Gly-X-Gly in an ensemble of 30 random conformations. Residues are considered to be solvent exposed if the ratio value exceeds 50% and to be buried if the ratio is less than 20%, marked as ''o'' (for ''out'') and ''i'' (for ''in'') respectively (Table 4).

Residues that are buried in the X-ray structure (Val^{87}, Phe^{90}, Asn^{92}, Thr^{95}) remain buried in the lowest energy conformations, while minor changes are evident in Asn (in position −3) and Pro^{96}. It is evident that no major conformational change occurs and we can use the conformation of the peptide obtained from the X-ray structure as a realistic representative of the MD ensemble for comparison with the conformations of the antagonistic peptides.

Table 4
Buried (i) and exposed (o) residues of the MBP ligand in the X-ray structure and the ten frames with the lowest energy after MD simulation. A blank entry indicates the ratio of side-chain surface area to "random coil" value is between 20% and 50%

	X-ray	1	2	3	4	5	6	7	8	9	10
Glu^{83}	o	o	o	o	o	o	o	o	o	o	o
Asn^{84}		o				o				o	o
Pro^{85}	o				o		o	o	o		
Val^{86}		o	o	o	o	o		o	o	o	
Val^{87}	i	i	i	i	i	i	i	i	i	i	i
His^{88}	o				o						o
Phe^{89}		i									
Phe^{90}	i	i	i	i	i	i	I	i	i	i	i
Lys^{91}	o	o	o	o	o	o	o	o	o	o	o
Asn^{92}	i	i	i	i	i	i	i	i	i	i	i
Ile^{93}			i	i	i			i			
Val^{94}	o	o	o	o	o	o	o	o	o	o	o
Thr^{95}	i	i	i	i	i	i	i	i	i	i	i
Pro^{96}		o	o				o		o	o	

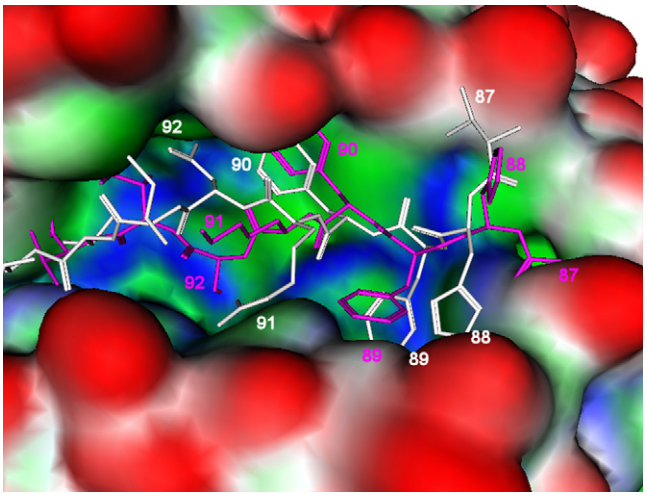

Fig. 3. The lowest energy structure of the complex of [Arg^{91}, Ala^{96}] $MBP_{87–99}$ (white) - HLA-DR2b, where the receptor is modelled as a surface. The X-ray structure of $MBP_{83–96}$ (purple) has been superimposed.

3.3. Molecular dynamics of [Arg^{91}, Ala^{96}] $MBP_{87–99}$ complexed with HLA-DR2b

In previous work [30] we proposed an active conformation of [Arg^{91}, Ala^{96}] $MBP_{87–99}$ using a combination of NMR and MD studies. The proposed bioactive conformation was used as the starting point of MD simulation of the [Arg^{91}, Ala^{96}] $MBP_{87–99}$ – HLA-DR2b complex. The sequence similarities of the APLs with part of $MBP_{83–96}$ do not necessarily mean they have similar binding modes, since 4 N-terminal residues are missing that might induce a shift along the binding groove. The active site was calculated from the X-ray structure discussed above, using 4.5 Å proximity around the native ligand, extended to the residues whose atoms were involved. The bioactive conformation was placed in it by superimposing it with the native ligand and then deleting the latter. Keeping the protein fixed, the peptide was subjected to completely unrestrained energy minimization employing AMBER94 [59] force field, to let the peptide move freely and remove any steric clashes. The coordinates of the resulting system were used as an input for full MD simulation. The energy of the system at each time step of the trajectory was calculated and the ten lowest energy frames selected. These are shown as a superimposition in Fig. 2. The time values, starting from the system with lowest energy, are 1813 ps, 1533 ps, 1644 ps, 501 ps, 650 ps, 1490 ps, 1770 ps, 1685 ps, 557 ps, and 1047 ps (Cα RMSD: 1.208 Å).

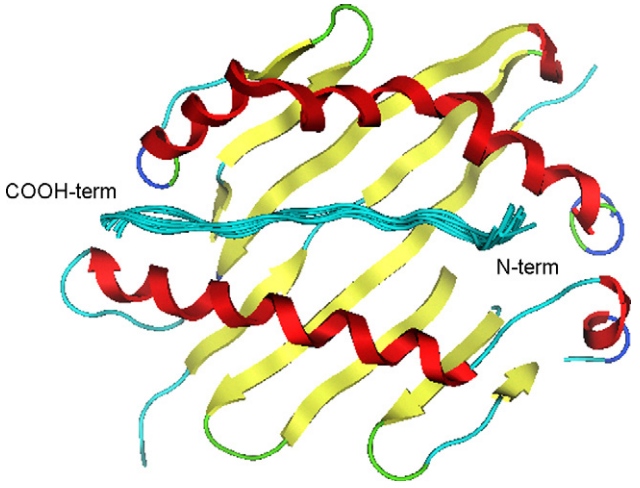

Fig. 2. The ten lowest energy frames after MD simulation of the [Arg^{91}, Ala^{96}] $MBP_{87–99}$ - HLA-DR2b complex. Both the peptides and the receptor are modelled as cartoon. Subunits α2 and β2 of the receptor are omitted for clarity.

Fig. 3 shows the lowest energy structure, where the receptor is shown as the Gauss–Connolly surface of the MOE software, and the peptide is shown in white. The sequence 83–96 of the peptide from the X-ray structure has been superimposed (shown in purple) for a better understanding of the changes in the conformation.

Large conformational differences between the APL and the native ligand are evident in Fig. 3. Val^{87} in the N-terminus is no longer sheltered in a hydrophobic pocket, but is exposed to the solvent. Residues His^{88} and Phe^{89}, complexed with the TCR in the X-ray structure, are no longer prominent and solvent exposed, and hence are not available to interact with the TCR. The phenyl ring of Phe^{90} still occupies pocket P4 as in the X-ray structure. There is a clear change in the backbone at the position of residues 91 and 92, causing a shift in the residues that serve as anchors to the receptor pockets. Asn^{92} remains buried in P6, but Ile^{93} no longer occupies a pocket. Val^{94} now appears to occupy the pocket P7, and Ala^{96} occupies P9, since Thr^{95} that occupies P9 in the X-ray structure is no longer buried.

SASA was again calculated for the ten low energy structures, and buried and exposed residues of the peptides were identified (Table 5). The highlighted rows show the major differences from the native peptide. We can see that whereas primary anchor Phe^{90} in P4 and secondary anchor Asn^{92} in P6 are similar to the crystal structure, secondary anchors in P7 and P9 have shifted due to the substitutions of $Lys^{91} \rightarrow Arg^{91}$ and $Pro^{96} \rightarrow Ala^{96}$, as well as the truncation of the N-terminus of the native peptide. Val^{94} and Ala^{96} now occupy these pockets.

Table 5
Buried (i) and exposed (o) residues of the MBP ligand in the X-ray structure, and the ten lowest energy frames of [Arg^{91}, Ala^{96}] MBP$_{87–99}$. A blank entry indicates the ratio of side-chain surface area to ''random coil'' value is between 20% and 50%

	X-ray structure	[Arg^{91}, Ala^{96}] MBP$_{87-99}$ 1	2	3	4	5	6	7	8	9	10
Val^{87}	i				o			o	o	o	o
His^{88}	o										
Phe^{89}		i	i	i	i	i	i	i	i	i	i
Phe^{90}	i	i	i	i	i	i	i	i	i	i	i
Arg^{91}	(LYS) o				i						
Asn^{92}	i	i	i	i	i	i	i	i	i	i	i
Ile^{93}		o	o	o	o	o	o	o	o	o	o
Val^{94}	o	i	i	i	i	i	i	i	i	i	i
Thr^{95}	i	o		o						o	
Ala^{96}	-	i	i	i	i	i	i	i	i	i	i
Arg^{97}	-	o	o	o	o	o	o	o	o		
Thr^{98}	-	o		o			o	o	o		o
Pro^{99}	-		o	o	o	o				o	o

The changes in secondary structure induced a significant alteration: the first TCR contact Phe^{89} is buried in all ten low energy conformations, and even though second TCR contact His^{88} does not meet the ratio criterion for being classified as buried, it has a very different orientation with respect to the X-ray structure, as seen in Fig. 3.

Scoring.svl was again used to identify direct hydrogen bonds (Table 6) and other non-bonded intermolecular interactions (Table 7) between the peptide and the receptor in the lowest energy conformation. Comparison of this data with those for the native peptide, reveals that all hydrogen bonds previously formed between the N-terminus of the peptide and the receptor are absent, as well as all hydrogen bonds involving Asn^{92},

Table 6
Network of hydrogen bonds formed between [Arg^{91}, Ala^{96}] MBP$_{87–99}$ and HLA-DR2b. α and β are the chains of the receptor

Hydrogen		Bonds			
		Ligand atom	Protein atom	Relative strength (%)	Distance (Å)
H(N)	Phe^{90}	OE1	α Gln^{9}	86	2.9
O	Phe^{90}	H(NE2)	α Gln^{9}	16	3.4
O	Phe^{90}	H(ND2)	α Asn^{62}	27	3.5
O	Val^{94}	H(ND2)	α Asn^{69}	7	3.2
O	Thr^{95}	OH	β Tyr^{60}	47	2.6
H(N)	Ala^{96}	OD1	α Asn^{69}	84	2.9
H(N)	Arg^{97}	OD1	β Asp^{57}	58	2.8
H(N)	Thr^{98}	OD1	β Asp^{57}	44	2.9

Table 7
Network of non-bonded intermolecular interactions between [Arg^{91}, Ala^{96}] MBP$_{87–99}$ and HLA-DR2b. α and β are the chains of the receptor

Ligand residue	Protein residue				
Val^{87}	β Thr^{77}	β Tyr^{78}	β His^{81}		
His^{88}	αPhe^{54}	α Glu^{55}			
Phe^{89}	α Gln^{9}	α Phe^{22}	α Phe^{24}	α Phe^{32}	
	α Val^{34}	α Phe^{54}	α Gly^{58}	α Ala^{59}	β Tyr^{78}
Phe^{90}	α Gln^{9}	α Phe^{24}	β Arg^{13}	β Phe^{26}	β Gln^{70}
	β Ala^{71}	β Ala^{73}	β Ala^{74}	β Thr^{77}	β Tyr^{78}
Arg^{91}	α Ala^{61}	β Gln^{70}			
Asn^{92}	β Tyr^{30}	β Ile^{67}	β Gln^{70}		
Ile^{93}	α Val^{65}	β Ile^{67}	β Gln^{70}		
Val^{94}	α Val^{65}	β Trp^{9}	β Pro^{11}	β Tyr^{30}	β Phe^{47}
	β Tyr^{60}	β Trp^{61}	β Ile^{67}	β Ala^{71}	
Thr^{95}	α Val^{65}	α Ala^{68}	β Tyr^{60}	β Trp^{61}	
Ala^{96}	α Ala^{68}	α Ile^{72}	α Met^{73}	β Trp^{9}	β Asp^{57}
	β Tyr^{60}	β Trp^{61}			
Arg^{97}	α Ile^{72}	β Tyr^{60}			
Thr^{98}	α Ile^{72}	β Pro^{56}	β Tyr^{60}		
Pro^{99}	α Ile^{72}	α Met^{73}	α Lys^{75}	α Arg^{76}	β Pro^{56}

Non-bonded intermolecular interactions between [Arg^{91},Ala^{96}] MBP$_{87–99}$ and HLA-DR2b.

whereas the hydrogen bonds for Phe^{90} are conserved. Residue Asn^{69} in chain α of HLA-DR2b forms hydrogen bonds with O Ile^{95} and NH Thr^{97} in the crystal structure; the same residue forms hydrogen bonds with O Val^{94} and NH Ala^{96} in the [Arg^{91}, Ala^{96}] MBP$_{87–99}$ antagonist, confirming the shift in the residues that occupy pockets P7 and P9.

Concerning the non-bonded interactions, the occupancy of P7 by Val^{94} is further shown by the fact that most of the residues with which it forms intermolecular contacts are those that Ile^{95} contacts in the native crystal structure. Three extra contacts with residues β Trp^{9}, β Pro^{11}, and β Ala^{71} are present, all buried in the protein's interior. Correspondingly, the buried residues in chains α and β of the protein that form P9 and contact Thr^{97} in the X-ray structure, now form contacts between Ala^{96} and the receptor in [Arg^{91}, Ala^{96}] MBP$_{87–99}$, reinforcing our finding that Ala^{96} is inserted into pocket P9.

The table of interactions shows another interesting aspect, namely alterations in the orientation of the residues in N-terminus of the peptide. Val^{87} contacts Tyr^{78} and His^{81} of the receptor's chain β, whereas these residues contact His^{90} in the X-ray structure. Thus it seems that Val^{87} has swapped places with His^{90}, with its side-chain now exposed to the solvent. Only Cα of His^{90} contacts α Phe^{54} in the X-ray structure, whereas all backbone and ring atoms of His^{88} are involved in the same interaction in the [Arg^{91}, Ala^{96}] MBP$_{87–99}$ – protein complex. α Phe^{54} is a buried residue protein, and this change reveals that His turns from a fully exposed residue in the native structure to an almost buried one in this APL complex. Also, Phe^{89} in the antagonist contacts exactly the same residues in the protein sequence as Phe^{91} in the native peptide does, but there are two extra contacts with residues Gln^{9} and Val^{34} of chain α. Both these residues are buried deep in the protein's interior. The

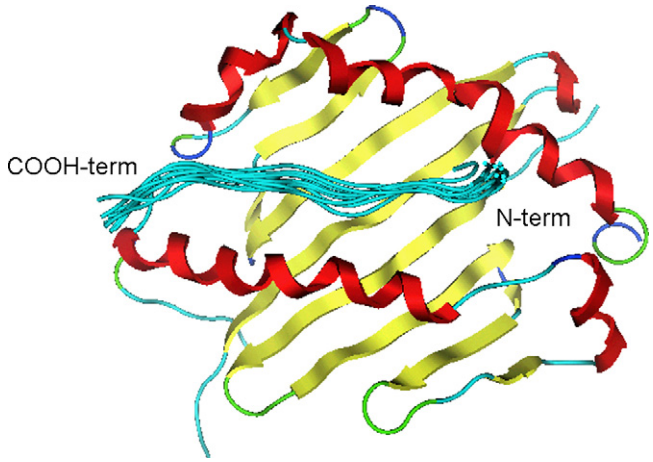

Fig. 4. The ten lowest energy frames after MD simulation of the [Ala^{91,96}] MBP$_{87–99}$ - HLA-DR2b complex. Both the peptides and the receptor are modelled as cartoon. Subunits α2 and β2 of the receptor have been omitted for clarity.

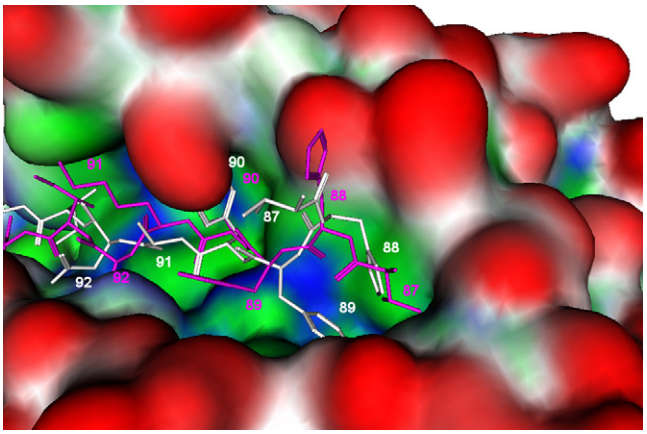

Fig. 5. The lowest energy complex of [Arg^{91}, Ala^{96}] MBP$_{87–99}$ (white) - HLA-DR2b, where the receptor has been modelled as a molecular surface. The sequence 83–96 of the peptide from the X-ray structure has been superimposed (purple).

result is that this residue now is overall buried, and not available for interactions with an approaching TCR molecule.

3.4. Molecular dynamics of [Ala^{91,96}] MBP$_{87–99}$ complexed with HLA-DR2b

In previous work [31] we established a putative bioactive conformation of [Ala^{91,96}] MBP$_{87–99}$ using the same method of NMR and MD studies. As before, this conformation has been used as the starting point for MD simulation of the peptide – HLA-DR2b complex. The same method, as described above, was followed for isolation of active site, constrained energy minimization, and transformation of the resulting coordinates into GROMACS input. The energy of the system at each time step of the obtained trajectory was calculated and the ten lowest energy frames selected (as shown in Fig. 4). Times values, starting from the system with lowest energy, are 1374 ps, 684 ps, 1176 ps, 1686 ps, 1525 ps, 1429 ps, 1455 ps, 386 ps, 1401 ps, and 1005 ps (Cα RMSD: 1.495 Å).

Fig. 5 shows the lowest energy complex, where the receptor is shown as a molecular surface, the peptide of interest in white, and the MBP$_{83–96}$ X-ray structure superimposed in purple. The backbone conformational flip found for [Arg^{91}, Ala^{96}] MBP$_{87–99}$ above is also present in the N-terminus of this peptide. Val^{87} has moved away from the hydrophobic pocket and is no longer buried, taking the place of His^{88} instead. The topology of the side chains of residues His^{88} and Phe^{89} is different than in [Arg^{91}, Ala^{96}] MBP$_{87–99}$, although once more the residues are no longer prominent and solvent exposed. In this case they both occupy the same pocket as Val^{87} did in the X-ray structure. Moreover, the phenyl ring of Phe^{90} remains in pocket P4.

Except this significant conformational change regarding the first three amino acids of [Arg^{91}, Ala^{96}] MBP$_{87–99}$, no major alteration takes place in the remaining sequence. Residues in positions 91, 94, and 96 (Ala, Val, and Ala respectively) remain exposed, and Asn^{92}, Ile^{93}, and Thr^{95} still occupy the pockets P6, P7, and P9 respectively. To quantify buried and exposed residues in the ten lower energy systems, SASA was calculated for the whole complexes: Table 8 shows the results.

The highlighted rows show the main differences from the native peptide, as described above. Primary anchor Phe^{90} in P4 and secondary anchors in P6, P7, and P9 remain the same as in the crystal structure. It seems that the substitution of Lys^{91} → Ala^{91} does not affect the backbone conformation as drastically as does Lys^{91} → Arg^{91}, probably due to the reduced size and thus minimization of intra-molecular and

Table 8
Buried (i) and exposed (o) residues of the MBP ligand in the X-ray structure and the ten lowest energy frames of [Ala^{91,96}] MBP$_{87–99}$. A blank entry indicates the ratio of side-chain surface area to "random coil" value is between 20% and 50%. See reference 58 for the numbering of the residues

	X-ray	[Ala^{91,96}] MBP$_{87-99}$									
	structure	1	2	3	4	5	6	7	8	9	10
Val^{87}	i	o	o	o	o	o	o	o	o	o	o
His^{88}	o	i		i	i	i	i	i	o	i	
Phe^{89}		i	i	i	i	i	i	i	i	i	i
Phe^{90}	i	i	i	i	i	i	i	i	i	i	i
Ala^{91}	(LYS) o	o	o	o	o	o	o	o		o	o
Asn^{92}	i	i	i	i	i	i	i	i	i	i	i
Ile^{93}		i	i	i	i	i	i	i	i	i	i
Val^{94}	o	o	o	o	o	o	o	o	o	o	o
Thr^{95}	i	i	i	i	i	i	i	i	i	i	i
Ala^{96}	-	o	o	o	o	o	o		o	o	o
Arg^{97}	-	o	o	o	o	o	o	o	o	o	o
Thr^{98}	-		i	i		i	i	i	o	i	
Pro^{99}	-	o	o	o	o	o	o	o	o	o	o

Table 9
Network of hydrogen bonds formed between [Ala^{91,96}] MBP$_{87-99}$ and HLA-DR2b. α and β are the chains of the receptor

Ligand atom		Protein atom		Relative strength (%)	Distance (Å)
Hydrogen bonds					
H(N)	Phe^{90}	OE1	α Gln^{9}	71	2.8
O	Phe^{90}	H(NE2)	α Gln^{9}	55	2.9
O	Phe^{90}	H(ND2)	α Asn^{62}	48	3.2
H(N)	Ala^{91}	OE1	β Gln^{70}	24	3.2
H(ND2)	Asn^{92}	OD2	α Asp66	44	3.1
O	Ile^{93}	H(ND2)	α Asn69	37	3.4
O	Val^{94}	H(NE1)	β Trp61	89	2.8
H(OG1)	Thr^{95}	OD1	α Asn69	64	2.8
H(N)	Ala^{96}	OD2	β Asp57	50	2.8
O	Thr^{98}	H(NZ)	α Lys75	21	3.3

inter-molecular interactions. Changes in secondary structure once more induce a significant change: the first TCR contact Phe^{89} is buried in all ten lower energy conformations, and the second TCR contact His^{88} meets the ratio criterion for being classified as buried in seven of them. Only in the conformation of the peptide corresponding to the system at t = 386 ps (rank 8) His^{88} is exposed.

3.5. Lowest energy conformation of [Ala^{91,96}] MBP$_{87-99}$ – HLA-DR2b complex

Scoring.svl was applied to the lowest energy complex. Direct hydrogen bonds identified between the peptide and the receptor are summarized in Table 9 and other non-bonded intermolecular interactions in Table 10. Comparison of Tables 6 and 9 reveals that all the hydrogen bonds for Phe^{90}, Ile^{93}, Val^{94}, and Thr^{95} are conserved, as well as one out of five for Asn^{92}.

Table 10
Network of non-bonded intermolecular interactions between [Ala^{91,96}] MBP$_{87-99}$ and HLA-DR2b. α and β are the chains of the receptor

Ligand residue	Protein residue				
Val^{87}	βThr^{77}				
His^{88}	βHis^{81}	β Val^{85}			
Phe^{89}	α Gln^{9}	α Phe^{22}	α Phe^{24}	α Phe^{32}	
	αSer^{53}	α Phe^{54}	α Glu^{55}	β Tyr^{78}	
Phe^{90}	α Gln^{9}	β Arg^{13}	β Phe^{26}	β Phe^{40}	
	βGln^{70}	β Ala^{71}	β Arg^{72}	β Ala^{74}	β Tyr^{78}
Ala91	βGln^{70}				
Asn^{92}	αAla^{61}	α Val^{65}			
Ile^{93}	αVal^{65}	β Trp^{9}	β Pro^{11}	β Tyr^{30}	β Phe^{47}
	βTrp^{61}	β Ile^{67}	β Ala^{71}		
Val^{94}	αVal^{65}	β Tyr^{60}	β Trp^{61}	β Ile^{67}	
Thr^{95}	αVal^{65}	α Asn^{69}	α Ile^{72}	β Trp^{9}	β Asp^{57}
	βTyr^{60}	β Trp^{61}			
Ala^{96}	α Ile^{72}	β Tyr^{60}			
Thr^{98}	α Ile^{72}	α Lys^{75}	α Arg^{76}		
Pro^{99}	αLys^{75}				

This is extra evidence that the topology of peptide backbone is similar to that of the X-ray structure. Here as well the hydrogen bonds between the first three residues in the amino acid sequence and the receptor are lost, due to the altered orientation.

The table of non-bonded interactions displays alterations in the orientation of residues in the N-terminus of this peptide. His^{88} contacts β Val^{85} of the receptor, a deeply buried residue that interacts with Val^{89} in the X-ray structure [36]. Also, the imidazole ring of His^{90} interacts with the exposed ring of β His^{81} in the X-ray structure, whereas in the [Ala^{91,96}] MBP$_{87-99}$ – protein complex it contacts the buried carbonyl group of the same residue. In common with [Arg^{91}, Ala^{96}] MBP$_{87-99}$ – protein complex, the system under study here also presents a swap between Val^{87} and His^{90}.

Phe^{89} in [Ala^{91,96}] MBP$_{87-99}$ contacts most of the same residues in the protein sequence as does the corresponding residue Phe^{91} in the native peptide. Two contacts with the exposed residues Ala^{61} and Asn^{62} of chain α are missing, and instead two new contacts form with residues α Gln^{9} and Ser^{53}. As mentioned before, α Gln^{9} is deep in the protein's interior. The interactions with Ser^{53} denote the change of the orientation of the phenylalanine ring, as Ser^{53} in the X-ray crystal is one of the residues forming the hydrophobic pocket P1.

For amino acids Asn^{92}, Ile^{93}, and Thr^{95} that are buried in pockets P6, P7, and P9 respectively, most residues forming the pockets are the same as in the X-ray structure and accordingly similar hydrophobic contacts are formed. Minor changes signify the motion of the receptor as well as the peptide during the dynamics simulation, in order to optimize interactions and result to more stable peptide – receptor complexes.

3.6. Orientation of TCR contacts His^{88} and Phe^{89} in the X ray structure of MBP$_{83-96}$ (agonist) with HLA-DR2b and the low energy complexes with the linear APLs (antagonists)

From the above structural analysis it is evident that the amino acids that serve as TCR contacts in the trimolecular complex of TCR-peptide-HLA (DR2b), *i.e.* His^{88} and Phe^{89}, have a different orientation in the antagonist analogues [Arg^{91}, Ala^{96}] MBP$_{87-99}$ and [Ala^{91,96}] MBP$_{87-99}$ compared with the agonist MBP$_{83-96}$. To quantify the relative change of the position of the imidazole His^{88} and phenyl Phe^{89} and Phe^{90} rings, we measured the angles and sides of the triangle formed by the centroids of the rings. In all cases, residue Phe^{90} was found to be positioned in the hydrophobic pocket P4, thus forming a common point of reference. These triangles are shown in Fig. 6, and the lengths of their sides and angles presented in Table 11. Fig. 7 shows a superimposition of the sequence His^{88} - Phe^{90} for the three molecules. This data confirm that the orientation of rings in His^{88} and Phe^{89} have altered substantially, whereas Phe^{90} tightly binds in P4 in all conformations. Both His^{88} and Phe^{89} shift towards the binding groove. The distance between their centroids is less than half of the corresponding distance in the X-ray structure.

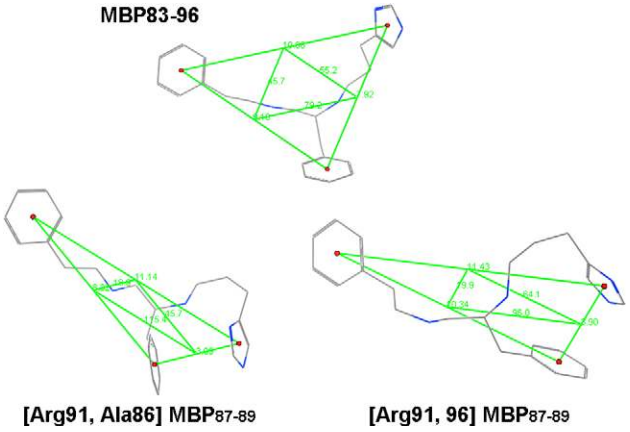

Fig. 6. Triangles formed by ring centroids of His[88], Phe[89] and Phe[90], for the X-ray structure of peptide $MBP_{83–96}$ and the lowest energy conformations of [Arg[91], Ala[96]] $MBP_{87–99}$ and [Ala[91,96]] $MBP_{87–99}$. Lengths of the sides and angles between the centroids are shown with green lines.

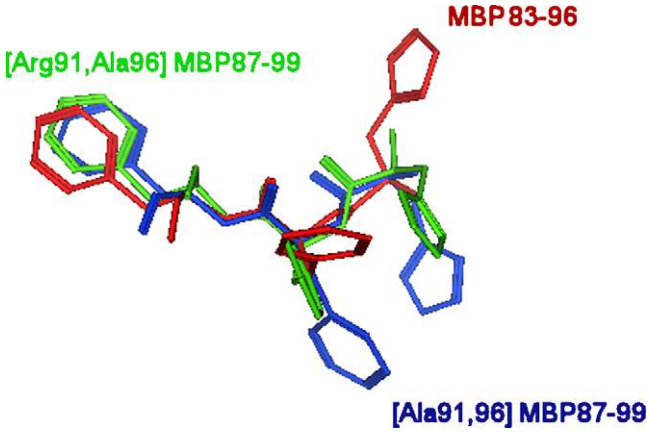

Fig. 7. Superimposition of His[88]- Phe[89]- Phe[90] for the X-ray structure of peptide $MBP_{83–96}$ and the lowest energy conformations of [Arg[91], Ala[96]] $MBP_{87–99}$ and [Ala[91,96]] $MBP_{87–99}$.

3.7. Possible mechanism of suppression of EAE by the APLs [Arg[91], Ala[96]] $MBP_{87–99}$ and [Ala[91,96]] $MBP_{87–99}$

The APLs [Arg[91], Ala[96]] $MBP_{87–99}$ and [Ala[91,96]] $MBP_{87–99}$ are active against EAE induced by guinea pig $MBP_{74–85}$ epitope. At the same time, [Arg[91], Ala[96]] $MBP_{87–99}$ [60] and the single Ala substituted $MBP_{87–99}$ in positions 91 and 96 [61] efficiently inhibited the proliferative response of human T cell clones isolated from patients with MS to the native peptide. Therefore, they were able to bind to human autoimmune TCRs, causing TCR antagonism. There is no X-ray structure of a TCR-APL-HLA (DR2b) trimolecular complex, which would allow us to study the TCR binding over the pMHC and to enlighten the antagonism shown by the APLs. Thus, we used the crystal structure of a human autoimmune TCR for comparison. To date, it was believed that this antagonistic activity is due to the substitution of the amino acids that serve as TCR anchors. Our results suggest that there is more to it.

X-ray studies have shown that the TCR from human autoimmune disease binds to the peptide - HLA-DR2b complex with an off-centre mechanism, which positions the CDR3 loops of the TCR over residues His[89] and Phe[90] of the N-terminus of the $MBP_{83–96}$ epitope [20]. Similarly, the trimolecular complex of TCR - peptide - HLA-DR2a [27] reveals that the TCR primarily recognizes the N-terminal portion of MBP peptide too. Both these crystal structures, the only ones using TCRs from human autoimmune disease to date, show a mode of binding different to that of antimicrobial and alloreactive TCRs, which bind over the peptide centre. DR2a and DR2b present completely different MBP residues to TCR as a result of a three-residue shift in peptide register [27], but it is striking that both human autoimmune TCRs primarily recognize the N-terminal, rather than central, portion of the peptide, as do all other TCRs. It seems that autoimmune TCRs focus on the N-terminal segment of the MBP peptide, favoring escape from the negative deletion in thymus.

In the antagonist APLs, our MD studies show that the side-chain imidazole and phenyl rings of residues His[89] and Phe[90] remain buried in MHC in all low energy conformations. These findings, along with the fact that the initial N-terminal four amino acids (Glu-Asn-Pro-Val) of the native peptide have been truncated, such as there cannot be an ‘‘arching up’’ of the CDR2 loop of the TCR to the MHC molecule, exclude the possibility of diagonal, off-centered binding of the TCR to the peptide-MHC complex, and may provide an explanation to the fact that [Arg[91], Ala[96]] $MBP_{87–99}$ and [Ala[91,96]] $MBP_{87–99}$ present antagonistic activity. The mode of binding of the TCR to the APL – MHC complex cannot be the diagonal manner seen for the native ligand, and must therefore be the conventional mode, *i.e.* centred over the peptide – MHC surface. This type of binding results in an optimal fit and could induce Th2 immune response and sufficient modification of the cytokine environment, altering the inflammatory cytokine profile [62].

Table 11
Geometries of triangles formed by centroids of rings of His[88], Phe[89] and Phe[90], for the X-ray structure of peptide $MBP_{83–96}$ and the lowest energy conformations of [Arg[91], Ala[96]] $MBP_{87–99}$ and [Ala[91,96]] $MBP_{87–99}$. d denotes the side length, c the ring centroid, and a the angle

	$MBP_{83–96}$	[Arg[91], Ala[96]] $MBP_{87–99}$	[Ala[91,96]] $MBP_{87–99}$
d (c88–c89)	7.92 Å	3.09 Å	3.90 Å
d (c89–c90)	9.10 Å	8.82 Å	10.34 Å
d (c90–c88)	10.88 Å	11.14 Å	11.43 Å
a (c88–c90–c89)	45.7°	18.9°	19.9°
a (c90–c88–c89)	55.2°	45.7°	64.1°
a (c90–c89–c88)	79.2°	115.4°	96°

4. Conclusion

The X-ray structure of a TCR isolated from a patient with relapsing-remitting MS reveals a different topology than that of previously determined antimicrobial TCR structures. It contacts only a small segment of the peptide, with its CDR3 loops over His[88] and Phe[89]. It is one of the best characterised TCRs from a human autoimmune disease and this aberrant binding

mode provides a possible explanation for the fact that in MS autoreactive T cells escape deletion in the thymus and attack self myelin [20]. A second recently determined X-ray of another human autoimmune TCR shows an off-centered mode of binding as well, although not so asymmetrical. It is shown that both human autoimmune TCRs primarily recognize the N-terminal residues.

We used the HLA-DR2b receptor to study the binding of two linear APLs, [Arg^{91}, Ala^{96}] $MBP_{87–99}$ and [$Ala^{91,96}$] $MBP_{87–99}$, in order to derive conclusions regarding their antagonistic activity. Full molecular dynamics studies in aqueous solvent were performed for the [Arg^{91}, Ala^{96}] $MBP_{87–99}$ – DR2b and [$Ala^{91,96}$] $MBP_{87–99}$ –DR2b complexes, with 2ns simulation time, using as an initial conformation for the peptides the putative active one as proposed by our earlier studies [30,31]. The X-ray structure of the peptide – HLA-DR2b complex was subjected to the same simulation.

In all three simulations, the complexes with the ten lower energies were studied, including calculation of SASA to determine whether residues are buried or exposed in each conformation. For the native X-ray structure complex, no major conformational changes occurred over the 2ns simulation. However, for the APLs it was found that once bound to the MHC, significant changes occur in the orientation of the amino acids that serve as TCR anchors (Figs. 6 and 7). In both APLs the TCR anchor Phe^{89} is buried in all conformers. TCR anchor His^{88} is buried in 7 of the conformations for the [$Ala^{91,96}$] $MBP_{87–99}$ - DR2 complex, and even though in the [Arg^{91}, Ala^{96}] $MBP_{87–99}$ - DR2 complex it does not meet the criterion for being classified as buried, it has a notably different orientation with respect to the X-ray structure. Both human autoimmune TCRs primarily recognize the N-terminal, unlike all other TCRs that bind over the central portion of the peptide. It is believed [21] that with that mode of binding the autoimmune TCRs favor escape from the negative deletion in thymus.

A possible mechanism of action can be proposed from these findings, combined with the fact that the APLs lack the N-terminal sequence that serves as the first contact for the TCR. The binding off the TCR over the pMHC would be in the conventional way, inducing an immune response against EAE. The molecular dynamics studies presented can therefore play a pivotal role in deciphering the mechanistic processes of this immunological response, providing detailed information on the molecular mechanisms underlying peptide-MHC recognition by TCRs.

Acknowledgements

Present work is supported by the Ministry of Development, Secretariat of Research and Technology of Greece (EPAN YB/76, PENED 2003: 03ED827).

References

[1] E.D. Mantzourani, T.M. Mavromoustakos, J.A. Platts, J.M. Matsoukas, T. Tselios, Structural requirements for binding of myelin basic protein (MBP) peptides to MHC II: Effects on immune regulation, Curr. Med. Chem. 12 (2005) 1521–1535.
[2] D.H. Margulies, Interactions of TCRs with MHC-peptide complexes: a quantitative basis for mechanistic models, Curr. Opin. Immunol. 9 (1997) 390.
[3] H. Von Boehmer, Positive and negative selection of the alpha beta T-cell repertoire in vivo, Curr. Opin. Immunol. 3 (1991) 210.
[4] R.B. Bell, J.W. Lindsey, R.A. Sobel, S. Hodgkinson, L. Steinman, T. Diverse, Cell receptor V beta gene usage in the central nervous system in experimental allergic encephalomyelitis, J. Immunol. 150 (1993) 4085.
[5] MHC sequence consortium. Complete sequence and gene map of a human MHC complex. Nature 1999, 401, 921.
[6] A. Compston, A. Coles, Multiple sclerosis, Lancet 359 (2002) 1221.
[7] E. Prat, R. Martin, The immunopathogenesis of MS, J. Rehab. Res. Devel. 39 (2002) 187–200.
[8] L. Barcellos, G. Thomson, Genetic analysis of MS in Europeans, J. Neuroimmunol. 143 (2003) 1–6.
[9] P.A. Muraro, M. Vergelli, M. Kalbus, D.E. Banks, J. Nagle, L.R. Tranquill, G.T. Nepom, W.E. Biddison, H.F. McFarland, R. Martin, Immunodominance of a low-affinity major histocompatibility complex-binding myelin basic protein epitope in HLA-DR4 subjects is associated with a restricted T cell receptor repertoire, J. Clin. Invest. 100 (1997) 339–349.
[10] D.R. Madden, The three-dimensional structure of peptide-MHC complexes, Annu. Rev. Immunol. 13 (1995) 587.
[11] L. Steinman, Assessment of animal models for MS and demyelinating disease in the design of rational therapy, Neuron 24 (1999) 511–514.
[12] S.S. Zamvil, L. Steinman, The T lymphocyte in experimental allergic encephalomyelitis, Annu. Rev. Immunol. 8 (1990) 579–621.
[13] K. Ota, M. Matsui, E.L. Milford, G.A. Mackin, H.L. Weiner, D.A. Hafler, T-cell recognition of an immunodominant myelin basic protein epitope in multiple sclerosis, Nature 346 (1990) 183–187.
[14] A. Valli, A. Sette, L. Kappos, C. Oseroff, J. Sidney, G. Miescher, M. Hochberger, E.D. Albert, L. Adorini, Binding of myelin basic protein peptides to human histocompatibility leukocyte antigen class II molecules and their recognition by T cells from multiple sclerosis patients, J. Clin. Invest. 91 (1993) 616–628.
[15] R. Martin, M.D. Howell, D. Jaraquemada, M. Flerlage, J. Richert, S. Brostoff, E.O. Long, D.E. McFarlin, H.F. McFarland, A myelin basic protein peptide is recognized by cytotoxic T cells in the context of four HLA-DR types associated with multiple sclerosis, J. Exp. Med. 173 (1991) 19–24.
[16] M.M. Davis, et al., Ligand recognition by αβ T-cell receptors, Annu. Rev. Immunol. 16 (1998) 523–544.
[17] M.G. Rudolph, I.A. Wilson, The specificity of TCR/pMHC interaction, Curr. Opin. Immunol. 14 (2002) 1043–1052.
[18] B.J. Hare, et al., Structure, specificity and CDR mobility of a class II restricted single-chain T-cell receptor, Nature Struct. Biol. 6 (1999) 574–581.
[19] B.E. Willcox, et al., TCR binding to peptide-MHC stabilizes a flexible recognition interface, Immunity 10 (1999) 357–365.
[20] K.J. Smith, J. Pyrdol, L. Gauthier, D.C. Wiley, K.W. Wucherpfennig, Crystal structure of HLA-DR2 (DRA*0101, DRB1*1501) complexed with a peptide from human myelin basic protein, J. Exp. Med. 188 (8) (1998) 1511.
[21] M. Hahn, M.J. Nicholson, J. Pyrdol, K.W. Wucherpfennig, Unconventional topology of self peptide-major histocompatibility complex binding by a human autoimmune T cell receptor, Nat. Immunol. 6 (5) (2005) 490–496.
[22] K.W. Wucherpfennig, A. Sette, S.S. Southwood, S.C. Oseroff, M. Matsui, J.L. Strominger, D.A. Haffler, Structural requirements for binding of an immunodominant myelin basic protein peptide to DR2 isotypes and for its recognition by human T cell clones, J. Exp. Med. 179 (1994) 279–290.
[23] K.W. Wucherpfennig, J. Zhang, C. Witek, M. Matsui, Y. Modabber, K. Ota, D.A. Hafler, Clonal expansion and persistence of human T cells specific for an immunodominant myelin basic protein peptide, J. Immunol. 152 (1994) 5581–5592.
[24] K.C. Garcia, M. Degano, L.R. Pease, M. Huang, P.A. Peterson, L. Teyton, I.A. Wilson, Structural basis of plasticity in T cell receptor recognition of a self peptide-MHC antigen, Science 279 (1998) 1166–1172.

[25] G.B. Stewat-Jones, A.J. McMichael, J.I. Bell, D.I. Stuart, E.Y. Jones, A structural basis for immunodominant human T cell receptor recognition, Nat. Immunol. 8 (2003) 403–411.
[26] J. Hennecke, A. Carfi, D.C. Wiley, Structure of a covalently stabilized complex of a human αβ T-cell receptor, influenza HA peptide and MHC class II molecule, HLA-DR1, EMBO J. 19 (2000) 5611–5624.
[27] Y. Li, Y. Huang, J. Lue, J.A. Quandt, R. Martin, R.A. Mariuzza, Structure of a human autoimmune TCR bound to a myelin basic protein self-peptide and a multiple sclerosis-associated MHC class II molecule, EMBO 24 (2005) 2968–2979.
[28] T. Tselios, I. Daliani, L. Probert, S. Deraos, E. Matsoukas, E. Roy, J. Pires, G. Moore, J. Matsoukas, Treatment of Experimental Allergic Encephalomyelitis (EAE) Induced by Myelin Basic Protein (MBP) Epitope 72–85 with Linear abd Cyclic Analogues of $MBP_{87–99}$, Bioorg. Med. Chem. 8 (2000) 1903–1909.
[29] Matsouka, E.M. Ph.D. thesis, Conformational studies of human $MBP_{87–99}$ associated with Multiple Sclerosis, 2001.
[30] E.D. Mantzourani, T.V. Tselios, S. Golič Grdadolnik, A. Brancale, J.A. Platts, J.M. Matsoukas, T.M. Mavromoustakos, A putative bioactive conformation for the altered peptide ligand of myelin basic protein and inhibitor of experimental autoimmune encephalomyelitis [Arg^{91}, Ala^{96}] $MBP_{87–99}$, J. Mol. Graph. Mod. 25/1 (2005) 17–29.
[31] E.D. Mantzourani, T.V. Tselios, S. Golič Grdadolnik, J.A. Platts, A. Brancale, G. Deraos, J.M. Matsoukas, T.M. Mavromoustakos, Comparison of proposed putative active conformations of linear altered peptide ligands of myelin basic protein epitope 87–99 by spectroscopic and modelling studies: the role of position 91 and 96 in T-cell receptor activation, J. Med. Chem. 49 (23) (2006) 6683–6691.
[32] M.C. Nicklaus, S. Wang, J.S. Driscoll, G.W. Milne, Conformational changes of small molecules binding to proteins, Bioorg. Med. Chem. 3 (4) (1995) 411–428.
[33] S. Wan, P. Coveney, D.R. Flower, Large scale molecular dynamics simulations of HLA-A*0201 complexed with a tumour-specific antigenic peptide: can the _3 and _2m domains be neglected? J. Comput. Chem. 25 (2004) 1803–1813.
[34] N. Karin, D.J. Mitchell, S. Brocke, N. Ling, L. Steinman, Reversal of experimental autoimmune encephalomyelitis by a soluble peptide variant of a myelin basic protein epitope: T cell receptor antagonism and reduction of interferon 3′ and tumor necrosis factor cr production, J. Exp. Med. 180 (1994) 2227–2237.
[35] The numbering of the peptide residues in the pdb structure ($MBP_{85–98}$) is according to Medline Unique Identifier (UID). The numbering in the APLs is different as the first residue of our epitope was labelled Val^{87}. Val^{87} of $MBP_{87–99}$ is equal to Val89 of $MBP_{85–98}$. For simplicity, in this paper we are referring to the pdb structure as $MBP_{83–96}$.
[36] H.J.C. Berendsen, D. Van der Spoel, R. Van Drunen, GROMACS: A message-passing parallel molecular dynamics implementation, Comp. Phys. Comm. 91 (1995) 43–56.
[37] E. Lindahl, B. Hess, D. Van der Spoel, Gromacs 3.0: a package for molecular simulation and trajectory analysis, J. Mol. Mod. 7 (2001) 306–317.
[38] W.F. Van Gunsteren, S.R. Billeter, A.A. Eising, P.H. Hünenberger, P. Krüger, A.E. Mark, W.R.P. Scott, I.G. Tironi, Biomolecular Simulation: the GROMOS96 manual and user guide., Zürich, Switzerland: Hochschulverlag AG an der ETH Zürich. (1996).
[39] R.W. Hockney, S.P.J. Goel, J.W. Eastwood, Quite high resolution computer models of a plasma J, Comp. Phys. 14 (1974) 148–158.
[40] B. Hess, H. Bekker, H.J.C. Berendsen, J.G. Fraaije, E.M. Lincs, A linear constraint solver for molecular simulations, J. Comp. Chem. 18 (1997) 1463–1472.
[41] W.F. Van Gunsteren, H.J.C. Berendsen, Gromos-87 manual. Biomos BV Nijenborgh 4, 9747 AG Groningen, The Netherlands (1987).
[42] A.R. Van Buuren, S.J. Marrink, H.J.C. Berendsen, A molecular dynamics study of the decane/water interface, J. Phys. Chem. 97 (1993) 9206–9212.
[43] W.L. Jorgensen, J. Chandrasekhar, J.D. Madura, R.W. Impey, M.L. Klein, Comparison of simple potential functions for simulating liquid water, J. Chem. Phys. 79 (1983) 926–935.
[44] A.R. Van Buuren, H.J.C. Berendsen, Molecular dynamics simulation of the stability of a 22 residue alpha-helix in water and 30% trifluoroethanol, Biopolymers 33 (1993) 1159–1166.
[45] H. Liu, F. M̈uller-Plathe, W.F. Van Gunsteren, A force field for liquid dimethyl sulfoxide and liquid proporties of liquid dimethyl sulfoxide calculated using molecular dynamics simulation, J. Am. Chem. Soc. 117 (1995) 4363–4366.
[46] D. Van der Spoel, A.R. Van Buuren, D.P. Tieleman, H.J.C. Berendsen, Molecular dynamics simulations of peptides from BPTI: a closer look at amide–aromatic interactions, J. Biomol. NMR 8 (1996) 229–238.
[47] P.E. Smith, W.F. Van Gunsteren, The viscosity of spc and spc/e water, Comp. Phys. Comm. 215 (1993) 315–318.
[48] H. Bekker, E.J. Dijkstra, M.K.R. Renardus, H.J.C. Berendsen, An efficient, box shape independent non-bonded force and virial algorithm for molecular dynamics, Mol. Sim. 14 (1995) 137–152.
[49] T. Darden, D. York, L. Pedersen, Particle mesh Ewald: An N-log(N) method for Ewald sums in large systems, J. Chem. Phys. 98 (1993) 10089–10092.
[50] U. Essmann, L. Perera, M.L. Berkowitz, T. Darden, H. Lee, L.G. Pedersen, A smooth particle mesh ewald potential, J. Chem. Phys. 103 (1995) 8577–8592.
[51] S. Nose, A molecular dynamics method for simulations in the canonical ensemble, Mol. Phys. 52 (1984) 255–268.
[52] W.G. Hoover, Canonical dynamics: equilibrium phase-space distributions, Phys. Rev. A 31 (1985) 1695–1697.
[53] Helix Computation and Visualization Facility http://www.helix.cf.ac.uk/.
[54] W. Humphrey, A. Dalke, K. Schulten, VMD—visual molecular dynamics, J. Mol. Graph. 14 (1996) 33–38.
[55] Chemical Computing Group Inc. 1010. Sherbrooke Street W, Suite 910; Montreal, Quebec; Canada H3A 2R7.
[56] SVL code exchange site for MOE Trade Mark user community http://svl.chemcomp.com/.
[57] R. Fraczkiewicz, W. Braun, J. Comp. Chem. 19 (1998) 319.
[58] R. Fraczkiewicz, W. Braun. A New Efficient Algorithm for Calculating Solvent Accessible Surface Areas of Macromolecules, ECCC3 1996, Northern Illinois Univ.
[59] W.D. Cornell, P. Cieplak, C.I. Bayly, I.R. Gould, K. Merz, D.M. Ferguson, D.C. Spellmeyer, T. Fox, J.W. Caldwell, P.A. Kollman, A second-generation force field for the simulation of proteins, nucleic acids, and organic molecules, J. Am. Chem. Soc. 117 (1995) 5179–5197.
[60] J. Matsoukas, V. Apostolopoulos, H. Kalbacher, A.M. Papini, T. Tselios, K. Chatzantoni, T. Biagioli, F. Lolli, S. Deraos, P. Papathanassopoulos, A. Troganis, E. Mantzourani, T. Mavromoustakos, A. Mouzaki, Design and synthesis of a novel potent myelin basic protein epitope 87–99 cyclic analogue: enhanced stability and biological properties of mimics render them a potentially new class of immunomodulators, J. Med. Chem. 48 (2005) 1470–1480.
[61] M. Vergelli, B. Hemmer, U. Utz, A. Vogt, M. Kalbus, N. Nanquill, P. Conlon, N. Ling, L. Steinman, H. McFarland, R. Martin, Differential activation of human autoreactive T cell clones by altered peptide ligands derived from myelin basic protein peptide (87–99), Eur. J. Immunol. 26 (1996) 2624–2634.
[62] M. Falcone, B.R. Bloom, J. Exp. Med. 185 (5) (1997) 901–907.